Optics Letters

Cross-polarization coupling of whispering-gallery modes due to the spin–orbit interaction of light

A. T. Rosenberger,[1,*] Elijah B. Dale,[1,2] Khoa V. Bui,[1,3] Erik K. Gonzales,[1,4] D. Ganta,[1,5] Limu Ke,[1] and Sreekul Raj Rajagopal[1]

[1]Department of Physics, Oklahoma State University, Stillwater, Oklahoma 74078, USA
[2]Radiance Technologies, 4950 Corporate Drive, Suite 125, Huntsville, Alabama 35805, USA
[3]School of Engineering Physics, Hanoi University of Science and Technology, Hanoi 100000, Vietnam
[4]Kirklind Global, Inc., 2719 M & K Lane, El Reno, Oklahoma 73036, USA
[5]School of Engineering, Texas A&M International University, Laredo, Texas 78041, USA
*Corresponding author: atr@okstate.edu

Received 10 June 2019; revised 19 July 2019; accepted 22 July 2019; posted 23 July 2019 (Doc. ID 369584); published 22 August 2019

Light can couple between two orthogonally polarized whispering-gallery modes of a microresonator; the effect is easily observable when those modes are frequency degenerate, and can result in coupled-mode induced transparency (CMIT). Experimental observations of CMIT show that the cross-polarization coupling (CPC) strength is typically 10^{-8}–10^{-7} per round trip. It is shown in this Letter that polarization rotation resulting from optical spin–orbit interaction through the experimentally realistic asymmetry of a microresonator about its equator can produce CPC with strengths in the same range as observed in experiments.

https://doi.org/10.1364/OL.44.004163

Two families of orthogonally polarized whispering-gallery modes (WGMs) exist within a dielectric microresonator. These are the transverse electric (TE) and transverse magnetic (TM) modes, which are, ideally, independent of each other. However, it is possible for light to couple between TE and TM modes in a non-ideal resonator. This cross-polarization coupling (CPC) produces observable effects if the two modes are frequency degenerate (co-resonant). We have found that if linearly polarized light is incident on the resonator and the throughput is polarization analyzed, WGMs of the incident polarization will appear as dips in the throughput power, and those of the orthogonal polarization will appear as peaks because of excitation by CPC. Observation of the throughput without polarization analysis can result in misinterpretation of the dip depth when CPC occurs. The observation [1–3] of coupled-mode induced transparency or attenuation (CMIT, CMIA) or Autler–Townes splitting (ATS) confirms that CPC is an intracavity process. Similar effects of polarization conversion can be observed without intracavity coupling [4–8], but effects such as CMIT require it, and we will use the term CPC to imply intracavity coupling. We emphasize that this is distinct from the polarization cross coupling of Nasir, *et al.* [8], which requires no CPC, just a misalignment of the input/detection polarization basis from the WGM basis.

Extensive experimental investigation has led us to the conclusion that polarization rotation is responsible for CPC. In this Letter, it is shown theoretically that polarization rotation in a slightly asymmetric microresonator leads to CPC with a strength that agrees with experimental CMIT/ATS results [2,3,9,10]. This effect is one manifestation of spin–orbit interaction of the light in a WGM.

Polarization rotation of guided waves due to asymmetries such as tilted sidewalls has long been known and studied [11–13]. It has been observed not only in waveguides but also in resonators [14–17]. Previous work has shown that such asymmetry-based polarization rotation is a result of optical spin–orbit interaction, or a Berry phase effect [18–20]. In these studies and the current work, these are geometrical effects; similar rotation of polarization can also be observed in structures made of birefringent material [21,22].

Here, we show that slight axial asymmetry of a WGM microresonator about its equator leads to CPC through polarization rotation in total internal reflection [23,24]. The interaction of spin and extrinsic orbital angular momentum [25] of light in a WGM results in a reflection phase shift that is different for the two circular polarizations, producing polarization rotation and thus CPC. The WGM is treated in the eikonal approximation [26,27], making one total reflection per wavelength propagation distance, and the mode asymmetry produces a slight polarization rotation with each reflection. Coupled-mode theory is then used to take into account the phase mismatch between the two orthogonally polarized WGMs and their spatial overlap. This is done for several representative pairs of orthogonally polarized co-resonant WGMs to get a quantitative estimate of the range of CPC strengths (probability of polarization change per round trip) that compares well with experimental observation [2,3,9,10].

Light in a WGM circulates in the equatorial plane of the microresonator, confined by total internal reflection. Because the dimensions of the resonator are orders of magnitude larger

than the wavelength of the light, a quasi-classical method, based on the eikonal approximation, gives a very good approximation to the exact WGM eigenfrequencies of the resonator [26,27]. Using this method, a mode is seen as being composed of rays that make m reflections per round trip, with the distance between reflections being one wavelength λ.

The orbital angular momentum of the WGM light circulating along the equator is in the z direction, along the resonator axis. After one reflection, the incident TE (s-polarized) field will produce a change in the TM (p-polarized) component, or vice versa, according to

$$dE_{\mathrm{TM}} = t_s' E_{\mathrm{TE}} \quad \text{or} \quad dE_{\mathrm{TE}} = -t_p' E_{\mathrm{TM}}, \tag{1}$$

where [23,24]

$$t_{s,p}' = \frac{2\pi\langle\beta_z\rangle}{m\beta_{\mathrm{TE,TM}}}. \tag{2}$$

Here, $\beta_{\mathrm{TE,TM}}$ is the propagation constant of the light in the incident WGM; for polarization rotation to occur, clearly its average axial component $\langle\beta_z\rangle$ must be nonzero, thus requiring asymmetry of the WGM about the equatorial plane. The rotation probability amplitude (per reflection) t_s' is proportional to the cotangent of the angle of incidence (π/m) and will be many orders of magnitude smaller than unity, so higher-order corrections from [23], including a complex term with phase equal to the very small s-p reflection phase difference, have been neglected.

In order to make a quantitative estimate of the CPC strength, the microresonator and its WGMs need to be specified. We have used microspheres and hollow bottle resonators (HBRs) [28–31] for studying CMIT [2,3,9,10]. Because of its various advantages such as usage for internal sensing and ease of strain tuning, the HBR is more convenient and will be considered here. A typical HBR is shown in Fig. 1.

The bulge in Fig. 1 is somewhat exaggerated; the HBRs that are typically used are made from capillaries of radius 160 μm, with a maximum bulge radius of $a = 175$ μm, and a wall thickness assumed to be 10 μm for purposes of mode calculations. A WGM in the HBR is characterized by three indices: m, as noted above, is the number of wavelengths in the equatorial circumference; p is the radial order, the number of radial intensity lobes; and q is the axial order, the number of nodes in the axial field profile. Because of the gentle axial curvature of the bulge, the wave equation approximately separates in cylindrical coordinates, and the amplitude of a WGM is given by

$$E_{mpq}(r,\varphi,z) = E_{\mathrm{TE,TM}} R_{mp}(r) Z_{mq}(z) \exp(im\varphi). \tag{3}$$

In Eq. (3), the radial function takes on different Bessel function forms in the three regions. Let $b = 165$ μm be the inner radius of the HBR and we have $R_{mp}(r)$ proportional to $J_m(n_1\beta_0 r)$ for $r < b$, to $J_m(n_2\beta_0 r) + c_{mp} Y_m(n_2\beta_0 r)$ for $b < r < a$, and to $H_m^{(1)}(n_3\beta_0 r)$ for $a < r$. Here, β_0 is the vacuum propagation constant, and n_1, n_2, and n_3 are the refractive indices in the three regions—interior, within the silica wall, and exterior, respectively. Given β_0 (within a narrow range), multiple solutions will exist for various combinations of m and p, having p radial lobes of intensity and mixing parameters c_{mp}. Let $\rho(z)$ be the outer radius of the resonator at axial position z, where $z = 0$ at the equator and $\rho(0) = a$. The shape of the bulge near the equator can be approximated as

$$\rho(z) = \rho(0)[1 + (\Delta k z)^2]^{-1/2}, \tag{4}$$

where Δk is an inverse length characterizing the change in radius with z. The profile of Eq. (4) means that the axial function $Z_{mq}(z/\sigma_z)$ has the approximate form of a Gaussian multiplied by a Hermite polynomial of order q, with $\sigma_z = (a/m\Delta k)^{1/2}$.

If the internal evanescent fraction is very small, the WGM is nearly the same as that of a solid bottle resonator; its frequency is given approximately by an expression [26,28,29,32] that allows the WGM's effective index of refraction to be found from

$$\frac{n_2}{n_{\mathrm{eff}}} \cong 1 + \frac{\alpha_p}{(2m^2)^{1/3}} - \frac{Ns}{m(N^2-1)^{1/2}} + \frac{3\alpha_p^2}{10(2m^2)^{2/3}} + \frac{N^3 s\left(\frac{2}{3}s^2 - 1\right)\alpha_p}{(2m^5)^{1/3}(N^2-1)^{3/2}} + \frac{\left(q+\frac{1}{2}\right)\Delta k a}{m}. \tag{5}$$

In Eq. (5), α_p is the negative of the pth zero of the Airy function, $N = n_2/n_3$, $s = 1$ for TE modes and $s = 1/N^2$ for TM modes, and n_{eff} is the effective index of the WGM, so that its propagation constant is $\beta = n_{\mathrm{eff}}\beta_0$.

The Fourier transform of the axial function is $Z_{mq}(\beta_z/\sigma_\beta)$, where $\sigma_\beta = (m\Delta k/a)^{1/2}$; this will result in a zero $\langle\beta_z\rangle$ if the WGM is symmetric about the equator. However, if the bulge is asymmetric, with slightly different curvature above and below the equator, the axial function can be approximated using Δk_+, σ_{z+}, and $\sigma_{\beta+}$ above the equator ($z > 0$) and Δk_-, σ_{z-}, and $\sigma_{\beta-}$ below the equator ($z < 0$). Then

$$\langle\beta_z\rangle = \int_0^\infty \beta_z Z_{mq}^2\left(\frac{\beta_z}{\sigma_{\beta+}}\right) d\beta_z - \int_0^\infty \beta_z Z_{mq}^2\left(\frac{\beta_z}{\sigma_{\beta-}}\right) d\beta_z \tag{6}$$

will be nonzero.

The effect of spatial overlap and phase mismatch can be accounted for by using the methods of coupled-mode theory [33] to write, for the amplitude coupled into the TM mode in one reflection,

$$\Delta E_{\mathrm{TM}} = t_s' E_{\mathrm{TE}} i C_{\mathrm{TETM}} \int_0^{2\pi/m} \exp(i\Delta\beta a\varphi) d\varphi, \tag{7}$$

where we have used $m\varphi = \beta a\varphi$ from Eq. (3), $\Delta\beta = \beta_{\mathrm{TE}} - \beta_{\mathrm{TM}} = (n_{\mathrm{eff\,TE}} - n_{\mathrm{eff\,TM}})\beta_0$, and

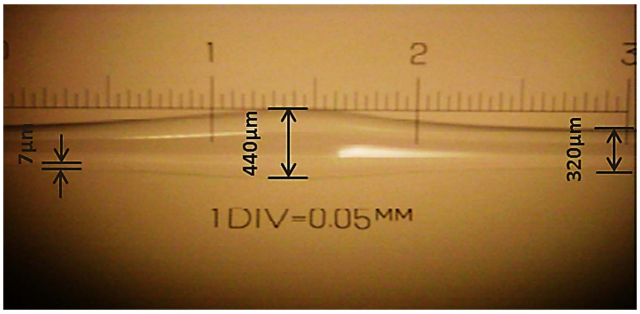

Fig. 1. Hollow bottle resonator (HBR). A fused-silica capillary is etched with HF solution to thin its walls, then heated and pressurized to create the bottle-shaped bulge. The z direction is along the capillary axis, and the equatorial plane is where the diameter is maximum. Note the slight asymmetry about the equatorial plane, resulting from unavoidable non-uniformity in heating while pressurizing.

$$C_{\mathrm{TETM}} = \frac{\beta_{\mathrm{TE}}^2 - \beta_{\mathrm{TM}}^2}{2\beta_{\mathrm{TM}}} \int_0^\infty R_{mp} R_{m'p'} r \mathrm{d}r \times \int_{-\infty}^{\infty} Z_{mq}\left(\frac{z}{\sigma_z}\right) Z_{m'q'}\left(\frac{z}{\sigma_z'}\right) \mathrm{d}z \tag{8}$$

in which the primed indices are for TE and the unprimed are for TM. Then the CPC strength resulting from the m' reflections in one round trip is denoted by

$$T_s = (m' t_s' C_{\mathrm{TETM}})^2 \frac{\sin^2\left(\frac{\Delta\beta}{2}\frac{2\pi a}{m'}\right)}{\left(\frac{\Delta\beta a}{2}\right)^2}. \tag{9}$$

In order to compare results of the analysis described above to experimentally determined values of CPC strength, we need to assume specific parameters of the HBR and of the two coupled WGMs to be used in the calculation. The input light of TE polarization is taken to have a vacuum wavelength of 1550 nm, where the refractive index of fused silica is $n_2 = 1.444$ (it is assumed that $n_1 = n_3 = 1$). At the equator, the outer radius of the HBR is $a = 175$ μm and the inner radius is $b = 165$ μm. Each WGM is characterized by the set (m, p, q, n_{eff}), and we take for TE the set (981, 3, 3, 1.3845) and for TM the set (959, 5, 5, 1.3578). Their radial intensity profiles are shown in Fig. 2.

The asymmetry assumed here is characterized by specifying the outer radius of the HBR at z positions 0.5 mm above and below the equator: $\rho(+0.5\ \mathrm{mm}) = 171.8$ μm, and $\rho(-0.5\ \mathrm{mm}) = 172.4$ μm. These typical values are estimated from measurements made on photographs such as Fig. 1. This results in slightly asymmetric axial intensity profiles, as shown in Fig. 3.

For these two modes, Eq. (9) gives a predicted strength for the CPC from this TE mode to this TM mode of $T_s = 2.82 \times 10^{-7}$. This value is near the upper limit of experimentally determined CPC strengths [2,3,9,10]; observed values range from about that upper limit to three orders of magnitude smaller, with typical values in the 10^{-8} range, such as the case shown in Fig. 4.

Since the size of the HBR is much larger than a wavelength ($m \gg 1$), it is not possible to precisely identify the mode numbers (m, p, q) of the WGMs that are coupled in an experiment

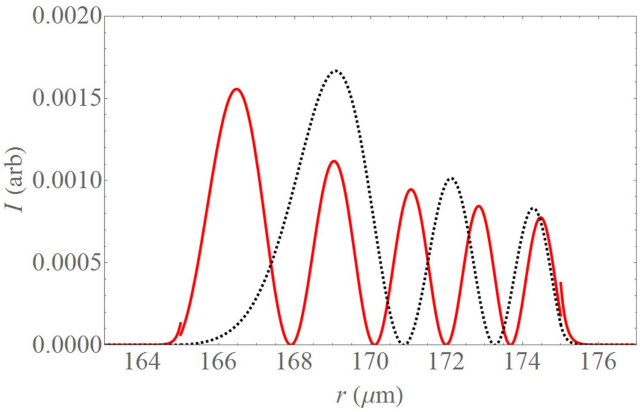

Fig. 2. Radial mode profiles for the two coupled WGMs excited by input light of 1550 nm vacuum wavelength. The outer radius of the HBR is at $r = a = 175$ μm; the inner radius is at $r = b = 165$ μm. Dashed black curve: TE, $p' = 3$. Solid red curve: TM, $p = 5$.

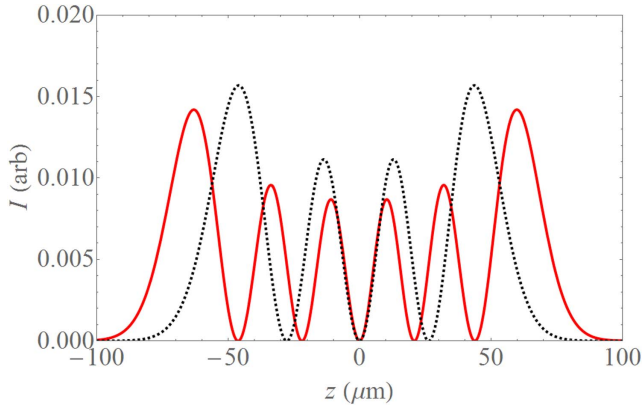

Fig. 3. Axial mode profiles for the two coupled WGMs excited by input light of 1550 nm vacuum wavelength. The point of maximum radius (equator) is at $z = 0$. Dashed black curve: TE, $q' = 3$. Solid red curve: TM, $q = 5$.

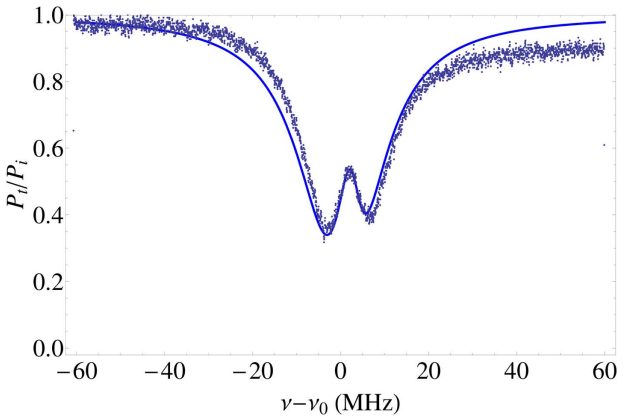

Fig. 4. CMIT with 200-μm-radius HBR [10]. Experimental (gray) and steady-state model (blue) throughput spectra. From the fit to the steady-state model, it is found that $T_s = 1.99 \times 10^{-8}$. A second method, using the response to input amplitude modulation, gives $T_s = 2.29 \times 10^{-8}$.

such as that in Fig. 4, but the mode numbers are not needed for the steady-state model. Based on the spectral density of observed WGMs, we estimate that their p values range from 1 to about 10 and their q values from 0 to about 10. Given these ranges, perhaps it is not surprising that the predicted T_s is near the upper observed limit, since the p and q values of the two WGMs used in the calculation are not very different and the resulting C_{TETM} is therefore larger than one found at random would be. The CPC strength has been calculated using the method described above for a few other TE/TM pairs of WGMs, and the results are shown in Table 1. The range of values agrees with the experimentally observed range. Note that T_p, for coupling from TM to TE is somewhat different from T_s, owing to the different axial extent of the two modes.

We have demonstrated that polarization rotation on total internal reflection can account for the strength of intracavity coupling of WGMs of orthogonal polarizations. Because of the small axial asymmetry, this is a manifestation of the optical

Table 1. Examples of Predicted CPC Strengths

TE (m, p, q)	TM (m, p, q)	T_s	T_p
981, 3, 3	959, 5, 5	2.82×10^{-7}	4.50×10^{-7}
1006, 1, 1	959, 5, 5	9.71×10^{-11}	3.57×10^{-10}
1006, 1, 1	981, 3, 3	3.83×10^{-8}	8.84×10^{-8}
992, 2, 2	970, 4, 4	1.12×10^{-7}	2.10×10^{-7}
1006, 1, 0	992, 2, 2	2.11×10^{-9}	1.28×10^{-8}

spin–orbit interaction. The predicted range of CPC strengths agrees with that found by two experimental methods using CMIT: steady-state model fit [2,3,9,10], as in Fig. 4, and input amplitude modulation response [9,10].

The calculated CPC strengths depend most strongly (variation by orders of magnitude) on the values of the mode overlap integrals such as C_{TETM}. These are not zero because the modes have different values of m. The dependences of the CPC strength on phase mismatch ($\Delta\beta$) and on the assumed asymmetry are much weaker (factors of less than 10). Questions that remain open concern the details of the effect of the mode numbers of the two WGMs and of the HBR wall thickness. If the wall is thinner, higher-order radial modes will have a significant internal evanescent component, affecting their effective refractive indices. Work is underway to derive an expression similar to Eq. (5) that accounts for the inner boundary as well as the outer.

REFERENCES

1. A. T. Rosenberger, Proc. SPIE **8636**, 863602 (2013).
2. K. V. Bui and A. T. Rosenberger, Proc. SPIE **9763**, 97630W (2016).
3. K. V. Bui and A. T. Rosenberger, preparing a manuscript to be called "Coupled mode induced transparency and attenuation resulting from cross-polarization coupling."
4. G. Guan and F. Vollmer, Appl. Phys. Lett. **86**, 121115 (2005).
5. H. Konishi, H. Fujiwara, S. Takeuchi, and K. Sasaki, Appl. Phys. Lett. **89**, 121107 (2006).
6. P. Bianucci, C. R. Fietz, J. W. Robertson, G. Shvets, and C.-K. Shih, Opt. Express **15**, 7000 (2007).
7. P. Bianucci, C. R. Fietz, J. W. Robertson, G. Shvets, and C.-K. Shih, Opt. Lett. **32**, 2224 (2007).
8. M. N. M. Nasir, S. B. Gorajoobi, G. S. Murugan, and M. N. Zervas, J. Opt. Soc. Am. B **36**, 705 (2019).
9. L. Ke, S. R. Rajagopal, and A. T. Rosenberger, Proc. SPIE **10904**, 109041T (2019).
10. L. Ke, S. R. Rajagopal, and A. T. Rosenberger, preparing a manuscript to be called "Dynamical determination of the strength of cross-polarization coupling in a whispering-gallery microresonator."
11. S.-T. Peng and A. A. Oliner, IEEE Trans. Microwave Theory Tech. **29**, 843 (1981).
12. A. A. Oliner, S.-T. Peng, T.-I. Hsu, and A. Sanchez, IEEE Trans. Microwave Theory Tech. **29**, 855 (1981).
13. W. W. Lui, T. Hirono, K. Yokoyama, and W.-P. Huang, J. Lightwave Technol. **16**, 929 (1998).
14. B. E. Little and S. T. Chu, IEEE Photon. Technol. Lett. **12**, 401 (2000).
15. F. Morichetti, A. Melloni, and M. Martinelli, J. Lightwave Technol. **24**, 573 (2006).
16. T. G. Nguyen, R. S. Tummidi, T. L. Koch, and A. Mitchell, Opt. Lett. **34**, 980 (2009).
17. D. A. Bykov and L. L. Doskolovich, Phys. Rev. A **97**, 013846 (2018).
18. H. G. L. Schwefel, A. D. Stone, and H. E. Tureci, J. Opt. Soc. Am. B **22**, 2295 (2005).
19. A. Morinaga, A. Monma, K. Honda, and M. Kitano, Phys. Rev. A **76**, 052109 (2007).
20. L. B. Ma, S. L. Li, V. M. Fomin, M. Hentschel, J. B. Götte, Y. Yin, M. R. Jorgensen, and O. G. Schmidt, Nat. Commun. **7**, 10983 (2016).
21. W. Weng and A. N. Luiten, Opt. Lett. **40**, 5431 (2015).
22. C. S. Werner, B. Sturman, E. Podivilov, S. K. Manjeshwar, K. Buse, and I. Breunig, Opt. Express **26**, 762 (2018).
23. C. Mi, S. Chen, X. Zhou, K. Tian, H. Luo, and S. Wen, Photon. Res. **5**, 92 (2017).
24. O. Hosten and P. Kwiat, Science **319**, 787 (2008).
25. K. Y. Bliokh, F. J. Rodriguez-Fortuño, F. Nori, and A. V. Zayats, Nat. Photonics **9**, 796 (2015).
26. M. L. Gorodetsky and A. E. Fomin, IEEE J. Sel. Top. Quantum Electron. **12**, 33 (2006).
27. D. Pluchon, B. Bêche, N. Huby, and E. Gaviot, Opt. Commun. **285**, 2247 (2012).
28. M. Sumetsky, Opt. Lett. **29**, 8 (2004).
29. G. S. Murugan, M. N. Petrovich, Y. Jung, J. S. Wilkinson, and M. N. Zervas, Opt. Express **19**, 20773 (2011).
30. R.-I. Stoian, K. V. Bui, and A. T. Rosenberger, J. Opt. **17**, 125011 (2015).
31. R.-I. Stoian, B. K. Lavine, and A. T. Rosenberger, Talanta **194**, 585 (2019).
32. N. M. Hanumegowda, C. J. Stica, B. C. Patel, I. White, and X. Fan, Appl. Phys. Lett. **87**, 201107 (2005).
33. B. E. A. Saleh and M. C. Teich, *Fundamentals of Photonics* (Wiley, 2007), p. 315.